Three-dimensional simulation of long-wavelength free-electron lasers with helical wiggler and ion-channel guiding

F. Jafari Bahman† and B. Maraghechi

Department of Physics, Amirkabir University of Technology, Tehran 15916-34311, *Iran*

(Received 11 May 2012; revised manuscript received 14 August 2012)

A three-dimensional simulation of a steady-state amplifier model of a long-wavelength free-electron laser (FEL) with realizable helical wiggler and ion-channel guiding is presented. The set of coupled nonlinear differential equations for electron orbits and fields of TE_{11} mode in a cylindrical waveguide are solved numerically by the Runge–Kutta algorithm with averages calculated by the Gaussian quadrature technique. Self-fields and space-charge effects are neglected, and the electron beam is assumed to be cold and slippage is ignored. The parameters correspond to the Compton regime. Evolution of the radiation power and growth rate along the wiggler is studied. Ion-channel density is chosen to obtain optimum efficiency. Simulations are preformed for the FEL operating in the neighborhood of 35 GHz and 16.5 GHz for the electron beam energies of 250 keV and 400 keV, respectively. The result of the saturated efficiency was found to be in good agreement with the simple estimation based on the phase-trapping model.

Keywords: free-electron laser, helical wiggler, ion-channel guiding

PACS: 41.60.Cr, 42.60.Jf, 42.65.Ky, 02.60.Cb **DOI:** 10.1088/1674-1056/22/7/074102

1. Introduction

The free-electron laser (FEL) is a high-power and tunable source of electromagnetic radiation over a wide range of frequencies from microwave to X-ray. The development of FELs in the microwave regime has some advantages. Since the energy of the electron beam is low, there is a considerable reduction in the cost of the accelerator. Also the requirements on the electron beam quality are less severe at long wavelengths. Furthermore, the dispersion characteristic of the waveguide resonator furnishes additional controlling parameters on the spectral characteristics of the emitted radiation. The possible application of high power millimeter and sub-millimeter waves from FELs include several technologies. These include fusion plasma applications, electron cyclotron discharges for generation of multi-charged ions and soft X-rays, high-frequency spectroscopy, advanced radar applications, and RF-drivers for multi-TeV linear colliders.[1] The high-power FEL microwave amplifiers are summarized in Refs. [2]–[4].

At long wavelengths, a waveguide and an axial magnetic field for the focusing purpose is normally employed. Alternatively, an ion-channel guiding can be used as a focusing method. In this method, a relativistic electron beam passes through a preionized plasma, ejects the electrons, and is guided by the positive ion core. Martin *et al.*[5] used this alternative method to transport a relativistic electron beam and Caporaso *et al.*[6] applied it in the advanced test accelerator. Takayama and Hiramatsu[7] were the first to suggest ion-channel guiding to be used in FEL and it was tested experimentally by Ozaki *et al.*[8] This technique was investigated via numerical simulation by Yu *et al.*[9] and by Jha and Wurtele.[10] The theoretical study of the FEL with helical wiggler and ion-channel guiding, in the low-gain-per-pass limit, shows substantial gain enhancement in one and three dimensions.[11–13] In Refs. [14] and [15], this problem has been studied in the high-gain regime in one dimension; however, analytical study of this configuration, in three dimensions, has not been done. Steady-state trajectories of electrons for this problem have been studied in one and three dimensions.[11–13,15–18]

The one-dimensional simulation of FEL in the presence of ion channels has been studied in Refs. [19]– [21]. In Ref. [10], an averaged three-dimensional simulation has been conducted, which allows for only some limited effects of an ion channel.

The purpose of the present investigation is to present the results of a three-dimensional simulation of an FEL with a helical wiggler and an ion channel, operating in the neighborhood of 35 GHz and 16.5 GHz. The electron beam and the electromagnetic radiation propagate through a conducting cylindrical waveguide. A set of nonlinear and coupled differential equations that self-consistently describe the evolution of both a collection of electrons and radiation are solved numerically. The parameters are in the high-gain Compton regime. Therefore, the space-charge fields are neglected. Since the TE_{11} mode was found to have the highest efficiency, and the TM and other TE modes were not considered. This problem with the ion channel replaced by an axial magnetic field was solved in Ref. [22]. Therefore, our presentation and notations are similar to theirs. In spite of similarities in presentation and notations, these two problems are considerably different in physics and formulation, as well as in results.

†Corresponding author. E-mail: jafary_bahman@yahoo.com

© 2013 Chinese Physical Society and IOP Publishing Ltd

The paper is organized as follows. In Section 2, the static fields of the wiggler and the ion channel, and the dynamical equations for the TE modes of radiation are presented. In Section 3, the nonlinear differential equations for the trajectory of electrons are introduced. In Section 4, numerical simulation results are given. Concluding remarks are made in Section 5.

2. Field equations

A three-dimensional nonlinear simulation of an FEL in amplifier mode is conducted to find the efficiency and the saturated power. The frequency corresponds to the microwave and the parameters correspond to the high-gain Compton regime. Therefore, the space-charge potential is small compared to the pondermotive potential and is neglected along with the self-fields of the electron beam. In this domain, electrons interact with each other only indirectly by coupling to the electromagnetic field (radiation) through the source term in the wave equation. The electron pulse is assumed to be long enough so that the slippage of the radiation over the electron beam is negligible and steady-state simulation with no time dependence can be used. In many simulation codes for an FEL like GENESIS,[23] the Lorentz force equations are reduced to a simplified form by means of an average over a wiggler period, whereas in the present method integration is over the complete equations of motion with no wiggler-averaged approximation. A slow time-scale formulation will be used, in which the electromagnetic wave is treated by a normal-mode analysis based upon a waveguide-mode expansion. Because of the expanded computational requirements, there are a limited number of particle-in-cell analyses of FEL amplifiers in three-dimensions.[24]

The realizable helical wiggler magnetic field generated by a bifilar helix can be expressed in cylindrical coordinates as

$$\boldsymbol{B}_{\mathrm{w}}(x) = 2B_{\mathrm{w}}(z)\left[\mathrm{I}_1'(\lambda)\cos\chi\boldsymbol{e}_r - \frac{1}{\lambda}\mathrm{I}_1(\lambda)\sin\chi\boldsymbol{e}_\theta + \mathrm{I}_1(\lambda)\sin\chi\boldsymbol{e}_z\right], \tag{1}$$

where $B_{\mathrm{w}}(z)$ denotes the wiggler amplitude, $k_{\mathrm{w}}(=2\pi/\lambda_{\mathrm{w}})$ is the wiggler wave number, $\lambda = k_{\mathrm{w}}r$, $\chi = \theta - k_{\mathrm{w}}z$, and I_n and I_n' denote the modified Bessel function of the first kind of order n and its derivative, respectively. It is assumed that the wiggler amplitude varies adiabatically to model the injection of the beam by means of tapered wiggler amplitude

$$B_{\mathrm{w}}(z) = \begin{cases} B_{\mathrm{w}}\sin^2\left[k_{\mathrm{w}}(z)/4N_{\mathrm{w}}\right], & 0 \le z \le N_{\mathrm{w}}\lambda_{\mathrm{w}}, \\ B_{\mathrm{w}}, & N_{\mathrm{w}}\lambda_{\mathrm{w}} < z \le z_0, \end{cases} \tag{2}$$

where N_{w} is the number of entry tapers of wiggler periods. The electrostatic field of ion channel is described as

$$\boldsymbol{E}_{\mathrm{i}}(x,y) = 2\pi e n_{\mathrm{i}}(x\boldsymbol{e}_x + y\boldsymbol{e}_y), \tag{3}$$

where n_{i} is the ion number density with positive charge e.

In the absence of a space-charge field, boundary conditions in the waveguide are satisfied by vector potential expansion in terms of the eigenmodes of the cylindrical waveguide. Therefore, the vector potential of the radiation field, for the TE modes, can be written as

$$\delta\boldsymbol{A}(x,t) = \sum_{\substack{l=0\\n=1}}^{\infty}\delta A_{ln}(z)\left[\frac{1}{\kappa_{ln}r}\mathrm{J}_l(\kappa_{ln}r)\sin\alpha_{ln}\boldsymbol{e}_r + \mathrm{J}_l'(\kappa_{ln}r)\cos\alpha_{ln}\boldsymbol{e}_\theta\right], \tag{4}$$

where $\alpha_{ln}(z)$, for frequency ω and wave number $k_{ln}(z)$, is defined as

$$\alpha_{ln}(z) = \int_0^z \mathrm{d}z' k_{ln}(z') + l\theta - \omega t, \tag{5}$$

J_l and J_l' are the Bessel function of the first kind and its derivative, and κ_{ln} is the cutoff wave number of waveguide modes. For the TE modes, $\kappa_{ln} \equiv x_{ln}'/R_{\mathrm{g}}$ with $\mathrm{J}_l'(x_{ln}') = 0$ and R_{g} is the radius of the waveguide

We can obtain equations for the slowly varying amplitude and wave number of each mode by substituting microscopic fields and source current in Maxwell's equations and following the procedure in Refs. [22] and [25]. By this procedure, dynamical equations for TE modes will be obtained as

$$\frac{\mathrm{d}}{\mathrm{d}\bar{z}}\delta a_{ln} \equiv \bar{\Gamma}_{ln}\delta a_{ln}, \tag{6}$$

$$\frac{\mathrm{d}}{\mathrm{d}\bar{z}}\bar{\Gamma}_{ln} \equiv -\left(\bar{\omega}^2 - \bar{k}_{ln}^2 - \bar{\kappa}_{ln}^2\right) + \frac{\bar{\omega}_{\mathrm{b}}^2 H_{ln}}{\delta a_{ln}}\left\langle\frac{\bar{v}_1 T_{ln}^{(+)} + \bar{v}_2 W_{ln}^{(+)}}{|\bar{v}_3|}\right\rangle, \tag{7}$$

$$\frac{\mathrm{d}}{\mathrm{d}\bar{z}}\bar{k}_{ln} \equiv -2\bar{k}_{ln}\bar{\Gamma}_{ln} + \frac{\bar{\omega}_{\mathrm{b}}^2 H_{ln}}{\delta a_{ln}}\left\langle\frac{\bar{v}_1 W_{ln}^{(-)} - \bar{v}_2 T_{ln}^{(-)}}{|\bar{v}_3|}\right\rangle, \tag{8}$$

where $\delta a_{ln} = e\delta A_{ln}/mc^2$, $\bar{\omega}_{\mathrm{b}}^2 = 4\pi n_{\mathrm{b}}e^2/mc^2k_{\mathrm{w}}^2$, and $\bar{v}_{1,2} = v_{1,2}/c$ are the transverse components of the electron velocity in rotating frame with wiggler defined by

$$\begin{cases} \boldsymbol{e}_1 = +\cos k_{\mathrm{w}}z\boldsymbol{e}_x + \sin k_{\mathrm{w}}z\boldsymbol{e}_y, \\ \boldsymbol{e}_2 = -\sin k_{\mathrm{w}}z\boldsymbol{e}_x + \cos k_{\mathrm{w}}z\boldsymbol{e}_y, \end{cases} \tag{9}$$

H_{ln}, $T_{ln}^{(\pm)}$, and $W_{ln}^{(\pm)}$ are given by

$$H_{ln} = \frac{x_{ln}'^2}{\left(x_{ln}'^2 - l^2\right)\mathrm{J}_l^2\left(x_{ln}'\right)}, \tag{10}$$

$$T_{ln}^{(\pm)} \equiv F_{ln}^{(\pm)}\sin\psi_{ln} + G_{ln}^{(\pm)}\cos\psi_{ln}, \tag{11}$$

$$W_{ln}^{(\pm)} \equiv F_{ln}^{(\mp)}\cos\psi_{ln} - G_{ln}^{(\mp)}\sin\psi_{ln}, \tag{12}$$

$$F_{ln}^{(\pm)} \equiv \mathrm{J}_{l-1}(\kappa_{ln}r)\cos(l-1)\chi \pm \mathrm{J}_{l+1}(\kappa_{ln}r)\cos(l+1)\chi, \tag{13}$$

$$G_{ln}^{(\pm)} \equiv \mathrm{J}_{l-1}(\kappa_{ln}r)\sin(l-1)\chi \pm \mathrm{J}_{l+1}(\kappa_{ln}r)\sin(l+1)\chi, \tag{14}$$

and the pondermotive phase is given by

$$\psi_{ln} \equiv \psi_0 + \int_0^z \mathrm{d}z' \left[k_{ln}(z') + lk_\mathrm{w} - \frac{\omega}{v_z} \right], \tag{15}$$

with $\psi_0 (= -\omega t_0)$ being the initial phase. Equation (6) may be considered as the definition of growth rate $\bar{\Gamma}_{ln}$ of the wave mode. Averages in the wave equations (7) and (8) represent the current formed by the moving electrons in nonlinear interaction with radiation. Derivation of dynamical equations (6)–(8) is presented in the appendix.

The average of beam electrons on axial phase and cross-section of waveguide is expressed as follows:

$$\langle (\ldots) \rangle = \frac{1}{2\pi A_\mathrm{g}} \int_{-\pi}^{\pi} \mathrm{d}\psi_0 \sigma(\psi_0) \times \iint_{A_\mathrm{g}} \mathrm{d}r_0 \mathrm{d}\theta_0 r_0 \sigma_\perp (r_0, \theta_0)(\ldots), \tag{16}$$

where (r_0, θ) is the initial transverse position of the electron that enters the interaction region at $z = 0$, $\sigma_\perp(r_0, \theta_0)$ and $\sigma(\psi)$ are the distribution of initial conditions, and A_g is the area of the cross section of the waveguide.

3. Electron orbit equations

The electron orbit equations can be obtained by substituting the fields into the Lorentz force equation. Equations for the normalized components of velocities in wiggler frames are

$$\begin{aligned} &\bar{v}_3 \frac{\mathrm{d}\bar{u}_1}{\mathrm{d}\bar{z}} \\ &= -\bar{\omega}_\mathrm{i}^2 (\bar{x}\cos\bar{z} + \bar{y}\sin\bar{z}) - \bar{u}_2 [2\bar{\Omega}_\mathrm{w} \mathrm{I}_1(\lambda)\sin\bar{\chi} - \bar{v}_3] \\ &\quad + \bar{\Omega}_\mathrm{w}\bar{u}_3 \mathrm{I}_2(\lambda)\sin(2\bar{\chi}) - \sum_{l,n} \frac{\delta a_{ln}}{2} \left[(\bar{\omega} - \bar{k}_{ln}\bar{v}_3) W_{ln}^{(-)} \right. \\ &\quad \left. - 2\bar{\kappa}_{ln}\bar{v}_2 \mathrm{J}_l(\bar{\kappa}_{ln}\bar{r})\cos\alpha_{ln} + \bar{\Gamma}_{ln}\bar{v}_3 T_{ln}^{(+)} \right], \end{aligned} \tag{17}$$

$$\begin{aligned} &\bar{v}_3 \frac{\mathrm{d}\bar{u}_2}{\mathrm{d}\bar{z}} \\ &= -\bar{\omega}_\mathrm{i}^2 (\bar{y}\cos\bar{z} - \bar{x}\sin\bar{z}) + \bar{u}_1 [2\bar{\Omega}_\mathrm{w} \mathrm{I}_1(\lambda)\sin\bar{\chi} - \bar{v}_3] \\ &\quad + \bar{\Omega}_\mathrm{w}\bar{u}_3 [\mathrm{I}_0(\lambda) + \mathrm{I}_2(\lambda)\cos(2\bar{\chi})] \\ &\quad + \sum_{l,n} \frac{\delta a_{ln}}{2} \left[(\bar{\omega} - \bar{k}_{ln}\bar{v}_3) T_{ln}^{(-)} \right. \\ &\quad \left. - 2\bar{\kappa}_{ln}\bar{v}_1 \mathrm{J}_l(\bar{\kappa}_{ln}\bar{r})\cos\alpha_{ln} + \bar{\Gamma}_{ln}\bar{v}_3 W_{ln}^{(+)} \right], \end{aligned} \tag{18}$$

$$\begin{aligned} &\bar{v}_3 \frac{\mathrm{d}\bar{u}_3}{\mathrm{d}\bar{z}} \\ &= \bar{\Omega}_\mathrm{w}\bar{u}_2 [\mathrm{I}_0(\lambda) + \mathrm{I}_2(\lambda)\cos(2\bar{\chi})] \\ &\quad - \bar{\Omega}_\mathrm{w} \mathrm{I}_1(\lambda)\sin(2\bar{\chi})\bar{u}_1 \\ &\quad - \sum_{l,n} \frac{\delta a_{ln}}{2} \left[\bar{k}_{ln} \left(\bar{v}_1 W_{ln}^{(-)} - \bar{v}_2 T_{ln}^{(-)} \right) \right. \\ &\quad \left. + \bar{\Gamma}_{ln} \left(\bar{v}_1 T_{ln}^{(+)} + \bar{v}_2 W_{ln}^{(+)} \right) \right], \end{aligned} \tag{19}$$

where $\bar{z} \equiv k_\mathrm{w} z$, $\bar{u} \equiv \gamma\bar{v}$, $\bar{v} \equiv v/c$, $\bar{\omega} \equiv \omega/ck_\mathrm{w}$, $\bar{k}_{ln} = k_{ln}/k_\mathrm{w}$, $\bar{\kappa}_{ln} = \kappa_{ln}/k_\mathrm{w}$, $\bar{\Gamma}_{ln} = \Gamma_{ln}/k_\mathrm{w}$, $\bar{\Omega}_\mathrm{w} = eB_\mathrm{w}/\gamma mc^2 k_\mathrm{w}$, and $\bar{\omega}_\mathrm{i}^2 = 2\pi n_\mathrm{i} e^2/mc^2 k_\mathrm{w}^2$. Equations for the transverse positions of the electron are

$$\bar{v}_3 \frac{\mathrm{d}\bar{x}}{\mathrm{d}\bar{z}} = \bar{v}_1\cos\bar{z} - \bar{v}_2\sin\bar{z}, \tag{20}$$

$$\bar{v}_3 \frac{\mathrm{d}\bar{y}}{\mathrm{d}\bar{z}} = \bar{v}_1\sin\bar{z} - \bar{v}_2\cos\bar{z}, \tag{21}$$

and for the pondermotive phase of electrons we have

$$\frac{\mathrm{d}\bar{\psi}_{ln}}{\mathrm{d}\bar{z}} = \bar{k}_{ln} + l - \frac{\bar{\omega}}{\bar{v}_3}. \tag{22}$$

Here, there are three equations for velocity, Eqs. (17)–(19), two equations for transverse positions of electrons, Eqs. (20) and (21), and one equation for pondermotive phase, Eq. (22). These six nonlinear differential equations that are coupled together show the evolution of velocity and location of each electron. Equations (6)–(8) show the evolution of amplitude and wave number of radiation. Thus, there are $6N^3$+3 equations with N^3 being the total number of electrons. These equations must be solved simultaneously by numerical means.

4. Results of simulation

We will use the fourth-order Runge–Kutta method to solve the above-mentioned set of coupled nonlinear deferential equations for FEL in the amplifier mode. To calculate the averages in the dynamical equations, N-th order Gaussian quadrature technique for each (r_0, θ_0, ψ_0) is used. We choose $N_r = N_\theta = N_\psi = 10$ for the number of electrons distributed in each coordinate, so the simulation can be performed for 1000 electrons. It needs to be mentioned that these 1000 macroparticles do not represent the actual number of electrons or the density of the electron beam. They are only used to find the averages in Eqs. (7) and (8).

The idealized case of a monoenergetic or cold beam is considered. It is assumed that a uniform and single energy electron beam with axial symmetry be injected into the system. There is no energy spread in this simulation. The electrons are picked within the ranges $-\pi \le \theta_0 \le \pi$, $-\pi \le \psi_0 \le \pi$, and $0 \le R_0 \le R_\mathrm{beam}$, where R_beam is the radius of the electron beam. The initial wave number is equivalent to vacuum value, $[k_{ln}(z=0) = (\omega^2/c^2 - \kappa_{ln}^2)^{1/2}]$. The initial growth rate for each mode is zero ($\Gamma_{ln}(z=0) = 0$), and we choose wiggler amplitude to increase from zero. Observe that the time-averaged pointing flux, P_{ln} for the waveguide modes is related to the field amplitude by the relation

$$P_{ln} = \frac{m^2c^4}{8e^2} \omega k_{ln} \frac{R_\mathrm{g}^2}{H_{ln}} \delta a_{ln}^2, \tag{23}$$

for the TE$_{ln}$ mode.

Steady-state helical orbits at the presence of helical wiggler and ion-channel guiding is

$$\boldsymbol{V} = v_{\rm w}\boldsymbol{e}_1 + v_{\parallel}\boldsymbol{e}_3. \tag{24}$$

For $v_{\rm w} = v_{\parallel}$ = constant, we have[17]

$$\beta_{\rm w} = \frac{2\bar{\Omega}_{\rm w}\beta_{\parallel}^2\left[{\rm I}_1(\lambda_0)/\lambda_0\right]}{\left[\bar{\omega}_{\rm i}^2 - \beta_{\parallel}^2 \pm 2\bar{\Omega}_{\rm w}\beta_{\parallel}{\rm I}_1(\lambda_0)\right]}, \tag{25}$$

where $\beta_{w,\parallel} = v_{w,\parallel}/c$, $\lambda_0 = \mp v_{\rm w}/v_{\parallel}$, and $\chi = \pm\pi/2$. Here, the upper and lower signs denote group-I and group-II orbits, respectively. Using the conservation law of energy we obtain

$$1 - \gamma^{-2} - \beta_{\parallel}^2 - \frac{4\bar{\Omega}_{\rm w}^2\beta_{\parallel}^4\left[{\rm I}_1(\lambda_0)/\lambda_0\right]^2}{\left[\bar{\omega}_{\rm i}^2 - \beta_{\parallel}^2 \pm 2\bar{\Omega}_{\rm w}\beta_{\parallel}{\rm I}_1(\lambda_0)\right]^2} = 0. \tag{26}$$

Therefore, there is a six-order polynomial for $\beta_{\parallel}$, as indicated in Fig. 1. The solution of this equation for positive $\beta_{\parallel}$ as a function of $\omega_{\rm i}/ck_{\rm w}$ shows the group-I and group-II steady-state helical trajectories for an electron in the presence of helical wiggler and ion channel. These two groups correspond to $\bar{\omega}_{\rm i}^2 < \beta_{\parallel}^2$ and $\bar{\omega}_{\rm i}^2 > \beta_{\parallel}^2$, respectively.[17]

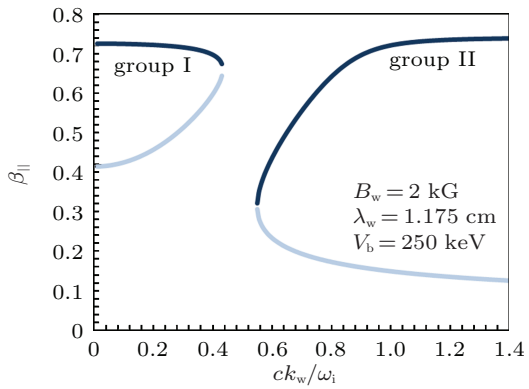


Fig. 1. (color online) Variation of the axial velocity as a function of ion-channel frequency for group-I and group-II ideal helical orbits.

As an example, we select an amplifier with a 35-GHz wide band that works at $\rm TE_{11}$ mode. The parameters are chose as: the amplitude of wiggler field is 2 kG, wavelength of the wiggler is 1.175 cm; electron beam has an energy of 250 keV, current of 35 A, and initial radius of 0.155 cm; waveguide radius is 0.36626 cm; input signal power is 10 W.

It must be noted that only the $\rm TE_{11}$ mode is chosen in this simulation because its cutoff frequency for the present parameter is closer to the input signal frequency $\omega/ck_{\rm w}$ chosen in this analysis, compared to the other modes with $l \neq 0$. The above waveguide radius is also chosen in such a way that the vacuum waveguide dispersion curve intersects the beam resonant line $\omega = (k_{ln} + k_{\rm w})v_{\parallel}$.

First, it is assumed that the axial energy spread is zero because of the initial state of the electron beam which is cold, monoenergetic, uniform, and has a flat-top density profile (i.e., $\sigma_{\perp} = \sigma_{\parallel} = 1$). The initial positions of electrons are chosen by means of a tenth-order Gaussian algorithm within the ranges of $-\pi \leq \theta_0 \leq \pi$, $-\pi \leq \psi_0 \leq \pi$, and $0 \leq R_0 \leq R_{\rm beam}$.

In Fig. 2, the initial axial phase space distribution (ψ_{ln}, ${\rm d}\psi_{ln}/{\rm d}z$) is shown. In fact, 1000 electrons are picked in a cylindrical space and each point in this figure shows the axial position of 100 electrons in phase space, which is the cross-sectional slice of the beam at this point. One of the cross-sectional slices of the beam at one dot of Fig. 2 is shown in Fig. 3. This sheet is composed of 100 electrons positioned at the cross section of the beam. The electrons are picked uniformly, but the nonuniformity in Figs. 2 and 3 are for the nonuniform weighting of a 10-point Gaussian weighting scheme. Although the initial distribution of the electrons is uniform, the subsequent motion of electrons in the presence of the radiation will be followed self-consistently and disrupt its uniformity.

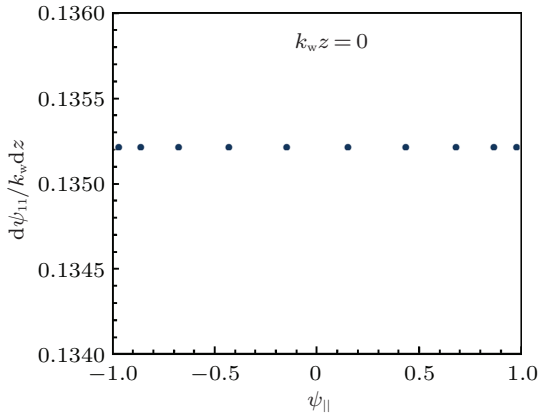


Fig. 2. (color online) Initial configuration of the axial phase space.

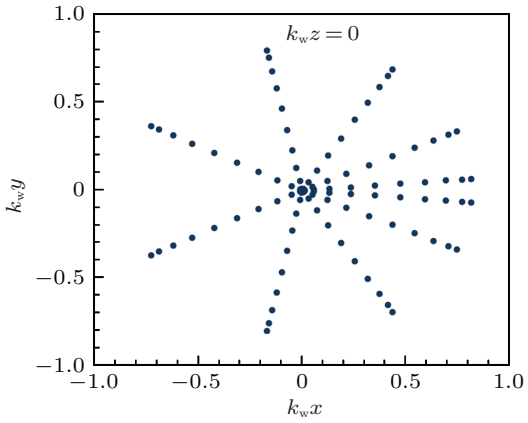


Fig. 3. (color online) Initial configuration of the cross section of the beam.

4.1. Group-I orbits

For the group-I orbits with $\omega_{\rm i}/ck_{\rm w} = 0.2$, we choose the input signal frequency $\omega/ck_{\rm w} = 1.3$, because for this combination, as we will see later, the efficiency is highest. In Fig. 4, evolution of the radiation power as a function of axial position is presented for group-I orbits with $\omega_{\rm i}/ck_{\rm w} = 0.2$. For

$k_w z < 67$, the power remains almost at its initial value (i.e., $P_{in} \simeq 10$ W). Power increases exponentially for $67 \leq k_w z \leq 330$ and continues to increase up to $k_w z \simeq 351$, which is the saturation point and the radiation amplitude does not increase any longer. Half of the electrons that are confined in pondermotive potential wells give energy to the wave, and the other half receives energy from the wave. Upon balance, saturation takes place. From this point on, radiation amplitude does not increase due to the reduced electron energy and the radiation amplitude decreases. We will have fluctuations beyond the saturation point. The region $0 < k_w z < 67$ corresponds to the small signal regime, exponential increase of power at $67 \leq k_w z \leq 290$ shows the linear regime, $290 \leq k_w z \leq 350$ is the nonlinear regime; and $k_w z \simeq 351$ is the saturation point with the saturation power of 1.79×10^6 W. We chose the normalized frequency at $\omega/ck_w = 1.3$ to obtain the best efficiency. As shown in Fig. 4, before $k_w z \simeq 67$, the growth rate is zero, and for $67 \leq k_w z \leq 290$ growth rate has a constant value, approximately equal to 0.02. This constant nonzero value for growth rate shows the linear regime, which indicates the exponential increase of power. Growth rate increases in the nonlinear region at $290 < k_w z < 330$ and decreases suddenly beyond $k_w z = 330$ reaching the zero growth rate at saturation point. Then, the growth rate decreases to $k_w z \simeq 351$ where it becomes zero and radiation saturates.

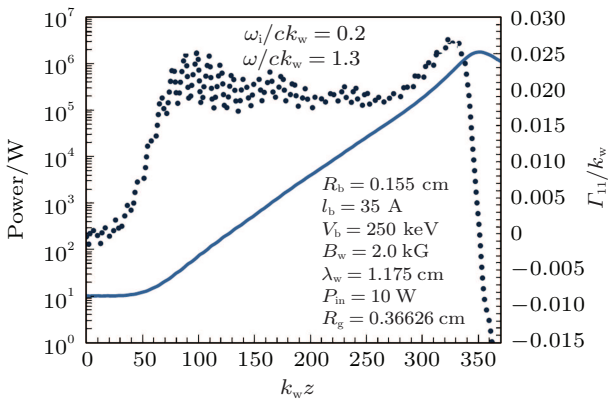


Fig. 4. (color online) Evolution of radiation power (solid line) and growth rate (dotted line) as a function of axial position, for a group-I orbit.

Spectrum of efficiency at saturation versus frequency for waveguide radius $R_g = 0.36626$ cm and $R_g = 0.37$ cm is shown in Fig. 5 for TE_{11} mode. For $R_g = 0.36626$ cm, maximum of efficiency is at 21.5% and takes place at $\omega/ck_w = 1.3$. The maximum efficiency is obtained at $\omega/ck_w = 1.2$ for $R_g = 0.37$ cm, which is slightly more than the first case. Dots on the curves represent the results of numerical simulation. The above efficiency of 21.5% is comparable with the result of Ref. [20] (i.e., 21.4%) where the ion channel is replaced by the axial magnetic field. Furthermore, our result is in good agreement with the simple estimation of efficiency based on the phase-trapping model[23] that yields the estimated efficiency of 23.3%.

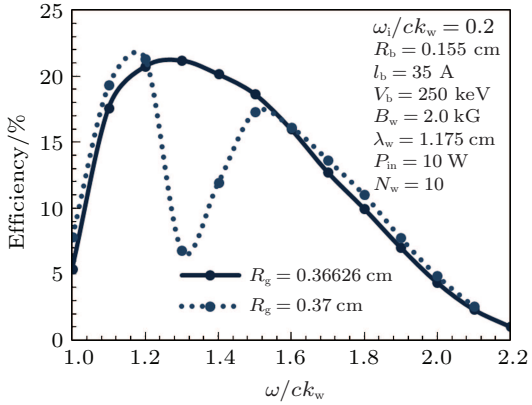


Fig. 5. (color online) Variation of efficiency with frequency for waveguide radius $R_g = 0.36626$ cm (solid line) and $R_g = 0.37$ cm (dotted line) for a group-I orbit.

4.2. Group-II orbits

In Fig. 6, evolution of the radiation power and growth rate as functions of axial position is presented for group-II orbits with $\omega_i/ck_w = 1.29$. In the small signal regime at $k_w z < 110$, power remains constant and in the linear regime at $110 < k_w z < 310$ power increases exponentially. Power continues to increase in the nonlinear regime at $310 < k_w z < 369$ until it saturates at $k_w z = 369$ with the saturated power of radiation equal to 5.92×10^5 W. It can be seen that compared with group-I orbits, saturation power is decreased and saturation length is increased. It can be seen in Fig. 4 that there is stronger fluctuations of growth rate in group-II orbits compared to the group-I orbits. In spite of these strong fluctuations, the average growth rate nicely describes all operating domains of the FEL.

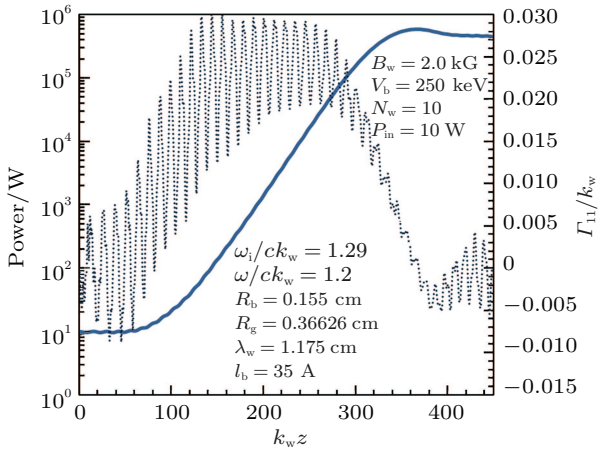


Fig. 6. (color online) Evolution of the radiation power (solid line) and growth rate (dotted line) as functions of the axial position for a group-II orbit.

The complete spectrum of interaction efficiency as a function of frequency is shown for TE_{11} mode in Fig. 7. The pick

of efficiency $\eta \simeq 6.75\%$ is at $\omega/ck_w = 1.2$. Dots on the curve represent the results of numerical simulation. It can be seen that efficiency in group-II orbits is reduced considerably compared with the group-I orbits.

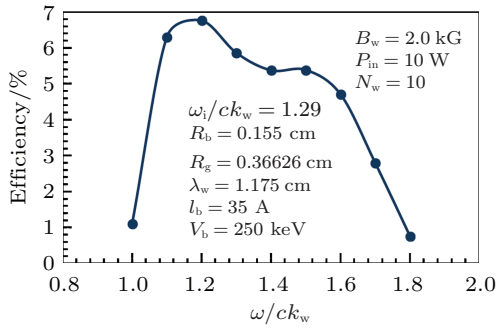


Fig. 7. (color online) Variation of efficiency with frequency for a group-II orbit.

In order to increase the efficiency in the group-II orbits, we first try to change the waveguide radius, but could not increase the efficiency. Then we try other ion-channel frequencies, but it turns out that the maximum efficiency takes places at $\omega_i/_w = 1.29$. The other convenient and important parameter that can be changed is the electron beam energy. Figure 8 shows the variation of axial velocity with normalized ion-channel frequency for $V_b = 400$ keV, $B_w = 1$ kG, and $\lambda_w = 2$ cm for group-I and group-II orbits. In Fig. 9, evolution of the radiation power (solid line) and growth rate (dotted line) as functions of the axial position is presented for group-II orbits with $\omega_i/_w = 0.88$. It is interesting to note that although there are strong fluctuations of growth rate, a strong saturated power of about 5.7×10^6 W and a very short distance to saturation of $k_w z \approx 183.9$ have been obtained. Figure 10 shows the efficiency versus the normalized frequency ω/ck_w for $V_b = 400$ keV, $R_g = 0.63$ cm and $R_g = 0.61$ cm. For $R_g = 0.63$ cm, the maximum efficiency of 30% takes places at $\omega/ck_w = 1$, while for $R_g = 0.61$ cm, the maximum efficiency is 26% at $\omega/ck_w = 1.1$. Therefore, by increasing the electron beam energy from 250 keV to 400 keV, we have been able to increase the efficiency considerably, for the group-II orbits, from 6.75% to 30%. The reason that group-II orbits require electron beam with high energy, compared to the group-I orbits, is that they experience higher ion-channel density and therefore, a stronger electrostatic field due to the ion channel. Interaction of this relatively strong electron field with the steady-state orbits of the electrons yields lower saturated power for low energy electrons of 250 keV. However, higher energy electrons of 400 keV pass through the electric field more easily, leading to higher saturated power and efficiency.

As it was mentioned earlier, notwithstanding the similarities, the simulation of an FEL with ion-channel guiding is quite different than that of the axial magnetic field. This can be viewed from different angles. For example, the steady-state orbits of electrons with ion channel, as described by Eq. (25), is different than that of the axial magnetic field because the focusing is due to the electrostatic field $\boldsymbol{E}_i$ in the former, while it is due to the magneto static field $\boldsymbol{B}_0$ in the latter. The electron orbit equations (17)–(19) are also different for the two cases, as the electrons are under influence of the electric field $\boldsymbol{E}_i$ in one case and the magnetic field $\boldsymbol{B}_0$ in the other case. In the presence of radiation, $\boldsymbol{E}_i$ does work on the electron, but $\boldsymbol{B}_0$ does not do any work. Furthermore, the simulation results are different, as one example shows in Fig. 11.

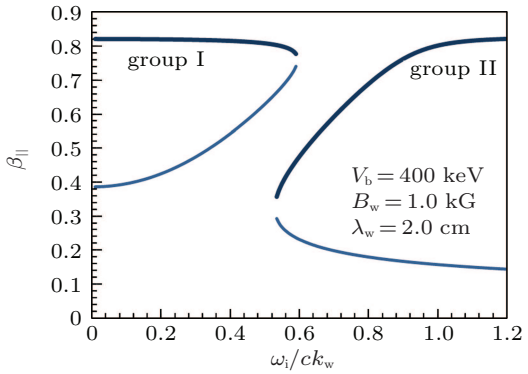


Fig. 8. (color online) Variation of the axial velocity as a function of ion-channel frequency for group-I and group-II ideal helical orbits.

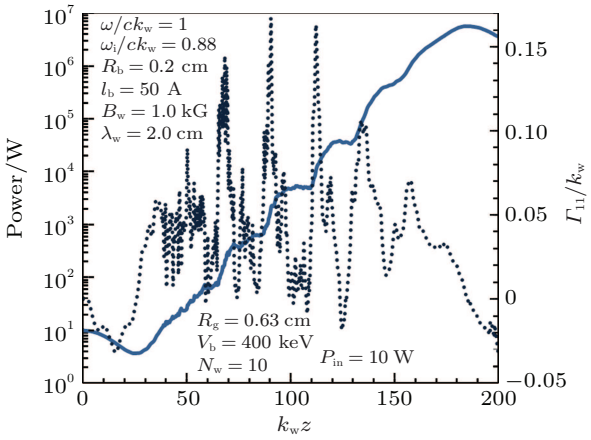


Fig. 9. (color online) Evolution of the radiation power (solid line) and growth rate (dotted line) as a function of axial position for a group-II orbit.

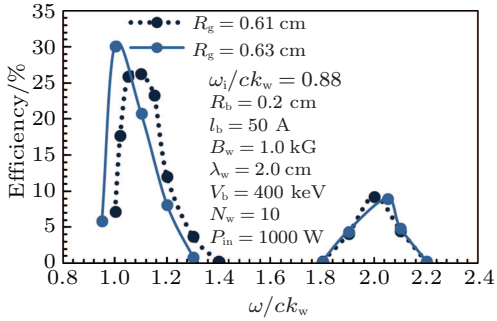


Fig. 10. (color online) Variation of efficiency with frequency for waveguide radius $R_g = 0.61$ cm (dotted line) and $R_g = 0.63$ cm (solid line).

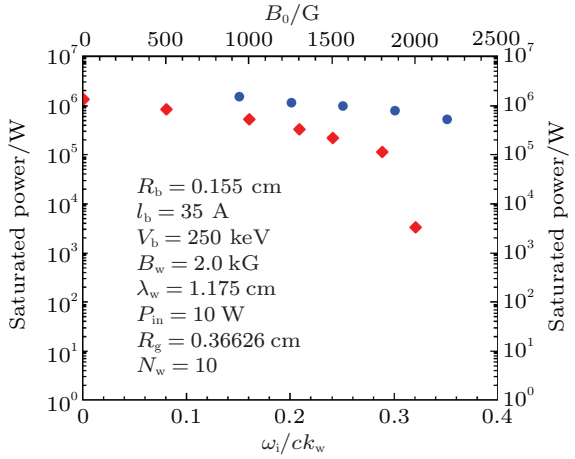


Fig. 11. (color online) Variation of the saturated power (dot) with ion-channel frequency and (diamond) with axial magnetic field.

5. Discussion and conclusion

In this work, we have presented the nonlinear simulation of an FEL amplifier in three dimensions. The arrangement consists of an electron beam with azimuthally symmetric circular cross section that is injected into a conducting circular waveguide. The electron beam is subject to a helical wiggler magnetic field and the electric field of an ion channel. Trajectories of a number of electrons that are initially distributed in three dimensions are followed self-consistently, and their influence on the evolution of the electromagnetic wave fields is calculated numerically. Only the TE_{11} mode that has the highest efficiency has been chosen to be resonant, and other modes with lower efficiency have not been studied. The parameters are in the Compton regime. Therefore, the space-charge fields are neglected.

The numerical technique and notations are similar to Refs. [22] and [25]. Since we did not have access to the original code, we first rewrote the original code, which was for the axial magnetic field, in place of the ion channel, and then modified it for the ion channel. In order to check its validity, we ran the code using the parameters and configuration in Ref. [22] and obtain identical results.

First, the energy of electron beam was chosen as 250 keV. The result of the numerical simulation showed the maximum efficiency of the group-I orbits as 21.5% and that of the group-II orbits as 6.75%. In order to increase the efficiency of the group-II orbits, a higher energy electron beam of 400 keV was also considered. We were able to optimize the parameters to obtain efficiency of 30% for the group-II orbits. It needs to be mentioned that there is no analytical calculation for the growth rate of the three dimensional problem that takes into account the boundary effects of the waveguide. Furthermore, due to the long-wavelength nature of microwave radiation, the result of the one-dimensional problem could not be used as a guidance to find the optimum parameters. Moreover, the efficiency that we obtained was normally not as large as we would like to obtain. By working on the parameters and optimizing them, we could obtain satisfactory efficiency such as 30%.

All of the peaks of the efficiency curves in this investigation correspond to the output frequency in the neighborhood of 35 GHz except for the two peaks at $\omega/_w = 1$ and 1.1, in Fig. 10, which is around 16.5 GHz. In the present analysis, electrons enter the interaction region uniform in energy and in space. This means that the electron beam is cold and is unbunched at the entrance into the wiggler. Similar problems with energy spread and prebunched electron beam require separate studies.

It is worth noting that an ion channel is a less expensive alternative to conventional focusing magnets because of the lower capital and running cost.[7]

Appendix A: Derivation of dynamical equations

Here, derivation of Eqs. (6)–(8) for the evolution of radiation is presented. The vector potential of the radiation field in the cylindrical waveguide, for the TE modes, can be written as

$$\delta A(x,t) = \sum_{\substack{l=0\\n=1}}^{\infty} \delta A_{ln}(z)\left[\frac{1}{\kappa_{ln}r}\mathrm{J}_l(\kappa_{ln}r)\sin\alpha_{ln}\boldsymbol{e}_r + \mathrm{J}_l'(\kappa_{ln}r)\cos\alpha_{ln}\boldsymbol{e}_\theta\right], \tag{A1}$$

where $\alpha_{ln}(z)$, for frequency ω and wave number $k_{ln}(z)$, is defined as

$$\alpha_{ln}(z) = \int_0^z \mathrm{d}z' k_{ln}(z') + l\theta - \omega t. \tag{A2}$$

Here, J_l and J_l' are the Bessel function of the first kind and its derivative, and κ_{ln} is the cutoff wave number of waveguide modes. For the TE modes, $\kappa_{ln} = x'_{ln}/R_g$ with $\mathrm{J}_l'(x'_{ln}) = 0$, and R_g is the radius of the waveguide. Substituting waveguide mode, Eq. (A1), into the Maxwell equations, we have

$$-\frac{4\pi e}{mc^3}\delta\bar{\mathrm{J}}_r = \sum_{l,n}\frac{\mathrm{J}_l(\kappa_{ln}r)}{\kappa_{ln}r}\left[\left(\frac{\mathrm{d}^2}{\mathrm{d}\bar{z}^2} + \bar{\omega}^2 - \bar{k}_{ln}^2 - \bar{\kappa}_{ln}^2\right)\delta a_{ln} \times \sin\alpha_{ln} + 2\bar{k}_{ln}^{1/2}\frac{\mathrm{d}}{\mathrm{d}\bar{z}}\left(\bar{k}_{ln}^{1/2}\delta a_{ln}\right)\cos\alpha_{ln}\right], \tag{A3}$$

and

$$-\frac{4\pi e}{mc^3}\delta\bar{\mathrm{J}}_\theta = \sum_{l,n}\mathrm{J}_l'(\kappa_{ln}r)\left[\left(\frac{\mathrm{d}^2}{\mathrm{d}\bar{z}^2} + \bar{\omega}^2 - \bar{k}_{ln}^2 - \bar{\kappa}_{ln}^2\right)\delta a_{ln} \times \cos\alpha_{ln} + 2\bar{k}_{ln}^{1/2}\frac{\mathrm{d}}{\mathrm{d}\bar{z}}\left(\bar{k}_{ln}^{1/2}\delta a_{ln}\right)\sin\alpha_{ln}\right], \tag{A4}$$

where $\delta a_{ln} = e\delta A_{ln}/mc^2$, $\bar{z} \equiv k_w z$ $\beta \equiv v/c$ $\bar{\omega} \equiv \omega/ck_w$ $\bar{k}_{ln} = k_{ln}/k_w$ and $\bar{\kappa}_{ln} = \kappa_{ln}/k_w$. By averaging over a

wave period and making use of the orthogonalization conditions over both the azimuthal angle and the radiation position such as

$$\int_{-\pi/\omega}^{\pi/\omega} \mathrm{d}t \sin\alpha_{lm} \sin\alpha_{ln} = \frac{2\pi}{\omega}\delta_{m,n}, \tag{A5}$$

$$\int_{-\pi/\omega}^{\pi/\omega} \mathrm{d}t \sin\alpha_{lm} \cos\alpha_{ln} = 0, \tag{A6}$$

and

$$\int_0^{R_\mathrm{g}} \mathrm{d}rr \left[\mathrm{J}_l'(\kappa_{ln}r)\mathrm{J}_l'(\kappa_{lm}r) + \frac{1}{\kappa_{ln}r}\frac{1}{\kappa_{lm}r}\mathrm{J}_l(\kappa_{ln}r)\mathrm{J}_l(\kappa_{lm}r)\right] = \frac{x_{ln}'^2 - l^2}{2\kappa_{ln}^2}\delta_{n,m}\mathrm{J}_l^2(x_{ln}'). \tag{A7}$$

The dynamical equations (A3) and (A4) take the following form in cylindrical coordinates:

$$\left(\frac{\mathrm{d}^2}{\mathrm{d}\bar{z}^2} + \bar{\omega}^2 - \bar{k}_{ln}^2 - \bar{\kappa}_{ln}^2\right)\delta a_{ln} = \frac{e}{mc^2}\frac{4\bar{\kappa}_{ln}^2}{c\left(x_{ln}'^2 - l^2\right)\mathrm{J}_l^2(x_{ln}')}\frac{\omega}{\pi}\int_{-\pi/\omega}^{\pi/\omega}\mathrm{d}t\int_0^{2\pi}\mathrm{d}\theta \times \int_0^{R_\mathrm{g}}\mathrm{d}rr\left\{\frac{\mathrm{J}_l(\kappa_{ln}r)}{\kappa_{ln}r}\sin\alpha_{ln}\delta\bar{\mathrm{J}}_r + \mathrm{J}_l'(\kappa_{ln}r)\cos\alpha_{ln}\delta\bar{\mathrm{J}}_\theta\right\}, \tag{A8}$$

$$-2\bar{k}_{ln}^{1/2}\frac{\mathrm{d}}{\mathrm{d}\bar{z}}\left(\bar{k}_{ln}^{1/2}\delta a_{ln}\right) = \frac{e}{mc^2}\frac{4\bar{\kappa}_{ln}^2}{c\left(x_{ln}'^2 - \bar{l}^2\right)\mathrm{J}_l^2(x_{ln}')}\frac{\omega}{\pi}\int_{-\pi/\omega}^{\pi/\omega}\mathrm{d}t\int_0^{2\pi}\mathrm{d}\theta \times \int_0^{R_\mathrm{g}}\mathrm{d}rr\left\{\frac{\mathrm{J}_l(\kappa_{ln}r)}{\kappa_{ln}r}\cos\alpha_{ln}\delta\bar{\mathrm{J}}_r - \mathrm{J}_l'(\kappa_{ln}r)\sin\alpha_{ln}\delta\bar{\mathrm{J}}_\theta\right\}. \tag{A9}$$

The final form for the dynamical equations is obtained by substitution of the source current. Therefore, the source current in three dimensions can be written as

$$\delta\boldsymbol{J}(\boldsymbol{x},t) = -en_\mathrm{b}v_{z0}\iint_{A_\mathrm{g}}\mathrm{d}x_0\mathrm{d}y_0\sigma_\perp(x_0,y_0) \times \int_{-T/2}^{T/2}\mathrm{d}t_0\sigma_\parallel(t_0)\boldsymbol{V}(z;x_0,y_0,t_0,\boldsymbol{p_0}) \times \frac{\delta\left[t-\tau(z;x_0,y_0,t_0,\boldsymbol{p_0})\right]}{|v_z(z;x_0,y_0,t_0,\boldsymbol{p_0})|}, \tag{A10}$$

where n_b is the ambient beam density, A_g is the area of the cross section of the waveguide, T is the duration of the electron beam pulse, v_{z0} is the initial axial velocity of the electron, (x_0, y_0) describes the cross-sectional position of the electron as it crosses the z=0 plane at t, $\sigma_\perp(x_0,y_0)$ is the cross-sectional distribution of the beam, $\sigma_\parallel(t_0)$ is the initial distribution in entry times, $\boldsymbol{p_0}$ is the initial momentum space distribution of the beam, and the Lagrangian time coordinate is defined as

$$\tau(z;x_0,y_0,t_0,\boldsymbol{p_0}) \equiv t_0 + \int_0^z \frac{dz'}{v_z(z';x_0,y_0,t_0,\boldsymbol{p_0})}. \tag{A11}$$

As a result, the dynamical equations for TE$_{ln}$ modes take the form of

$$\left[\frac{\mathrm{d}^2}{\mathrm{d}\bar{z}^2} + \left(\bar{\omega}^2 - \bar{k}_{ln}^2 - \bar{\kappa}_{ln}^2\right)\right]\delta a_{ln} = \bar{\omega}_\mathrm{b}^2 H_{ln}\left\langle\frac{\beta_1 T_{ln}^{(+)} + \beta_2 W_{ln}^{(+)}}{|\beta_3|}\right\rangle, \tag{A12}$$

$$2\bar{k}_{ln}^{1/2}\frac{\mathrm{d}}{\mathrm{d}\bar{z}}\left(\bar{k}_{ln}^{1/2}\delta a_{ln}\right) = \bar{\omega}_\mathrm{b}^2 H_{ln}\left\langle\frac{\beta_1 W_{ln}^{(-)} - \beta_2 T_{ln}^{(-)}}{|\beta_3|}\right\rangle. \tag{A13}$$

where $\bar{\omega}_\mathrm{b}^2 = 4\pi n_\mathrm{b}e^2/mc^2k_\mathrm{w}^2$, and H_{ln}, $T_{ln}^{(\pm)}$, and $W_{ln}^{(\pm)}$ are defined by Eqs. (10)–(14). The pondermotive phase is

$$\psi_{ln} \equiv \psi_0 + \int_0^z \mathrm{d}z'\left[k_{ln}(z') + lk_\mathrm{w} - \frac{\omega}{v_z}\right], \tag{A14}$$

with $\psi_0\,(=-\omega t_0)$ being the initial phase. The average of beam electrons on axial phase and cross-section of waveguide is expressed as follows:

$$\langle(\ldots)\rangle = \frac{1}{2\pi A_\mathrm{g}}\int_{-\pi}^{\pi}\mathrm{d}\psi_0\sigma(\psi_0) \times \iint_{A_\mathrm{g}}\mathrm{d}r_0\mathrm{d}\theta_0 r_0\sigma_\perp(r_0,\theta_0)(\ldots), \tag{A15}$$

where (r_0, θ) is the initial transverse position of the electron that enters the interaction region at $z = 0$, $\sigma_\perp(r_0, \theta)$ and $\sigma(\psi)$ are distribution of initial conditions

Equation $\bar{\Gamma}_{ln} = d(\ln\delta a_{ln})/d\bar{z}$ may be considered as the definition of growth rate $\bar{\Gamma}_\mathrm{ln}$ of the wave mode. Hence, using relation

$$\frac{\mathrm{d}^2}{\mathrm{d}\bar{z}^2}\delta a_{ln} = \frac{\mathrm{d}}{\mathrm{d}\bar{z}}\left(\bar{\Gamma}_{ln}\delta a_{ln}\right) = \delta a_{ln}\frac{\mathrm{d}}{\mathrm{d}\bar{z}}\bar{\Gamma}_{ln} + \bar{\Gamma}_{ln}\frac{\mathrm{d}}{\mathrm{d}\bar{z}}\delta a_{ln}, \tag{A16}$$

the dynamical equations for TE$_{ln}$ modes take the form of

$$\frac{\mathrm{d}}{\mathrm{d}\bar{z}}\delta a_{ln} \equiv \bar{\Gamma}_{ln}\delta a_{ln}, \tag{A17}$$

$$\frac{\mathrm{d}}{\mathrm{d}\bar{z}}\bar{\Gamma}_{ln} \equiv -\left(\bar{\omega}^2 - \bar{k}_{ln}^2 - \bar{\kappa}_{ln}^2\right) + \frac{\bar{\omega}_\mathrm{b}^2 H_{ln}}{\delta a_{ln}}\left\langle\frac{\bar{\nu}_1 T_{ln}^{(+)} + \bar{\nu}_2 W_{ln}^{(+)}}{|\bar{\nu}_3|}\right\rangle, \tag{A18}$$

$$\frac{\mathrm{d}}{\mathrm{d}\bar{z}}\bar{k}_{ln} \equiv -2\bar{k}_{ln}\bar{\Gamma}_{ln} + \frac{\bar{\omega}_\mathrm{b}^2 H_{ln}}{\delta a_{ln}}\left\langle\frac{\bar{\nu}_1 W_{ln}^{(-)} - \bar{\nu}_2 T_{ln}^{(-)}}{|\bar{\nu}_3|}\right\rangle. \tag{A19}$$

References

[1] Thumm M 2009 *Nucl. Instrum. Meth. Phys. Res. A* **483** 186
[2] Petelin M I 1999 *IEEE Trans. Plasma Sci.* PS-**27** 294
[3] Grantstein V L, Levush B, Danly B G and Parker R K *IEEE Trans. Plasma Sci.* PS-**25** 1322
[4] Freund H P and Neil G R 1999 *Proc. IEEE* **87** 782
[5] Martin W E, Caporaso G J, Fawley W M, Prosnitz D and Cole A G 1985 *Phys. Rev. Lett.* **54** 685

[6] Caporaso G J, Rainer F, Martin W E, Prone O S and Cole A G 1986 *Phys. Rev. Lett.* **57** 1591
[7] Takayama K and Hiramatsu S 1988 *Phys. Rev. A* **37** 173
[8] Ozaki T, Ebihara K, Hiramatsu S, Kishiro J, Monaka T, Takayama K and Whittum D H 1992 *Nucl. Instrum. Meth. Phys. Res. A* **318** 101
[9] Yu L H, Sessler A M and Whittum D H 1992 *Nucl. Instrum. Meth. Phys. Res. A* **318** 721
[10] Jha P and Wurtele J S 1993 1993 *Nucl. Instrum. Meth. Phys. Res. A* **331** 477
[11] Jha P and Kumar P 1996 *IEEE Trans. Plasma Sci.* **24** 1359
[12] Esmaeilzadeh M, Ebrahimi S, Siahian A, Willett J E and Willett L J 2005 *Phys. Plasmas* **12** 093103
[13] Mirzanejhad S and Asri M 2005 *Phys. Plasmas* **12** 093108
[14] Kordbacheh A A, Maraghechi B, Farokhi B and Willett J E 2005 *Phys. Plasmas* **12** 113106
[15] Jha P and Kumar P 1998 *Phys. Rev. E* **57** 2256
[16] Esmaeilzadeh M, Mehdian H and Willett J E 2001 *Phys. Rev. E* **65** 016501
[17] Mirzanejhad S and Asri M 2005 *Phys. Plasmas* **12** 093108
[18] Mirzanejhad S, Maraghechi P and Maraghechi B 2004 *Phys. Plasmas* **11** 3047
[19] Raghavi A, Ninno G D and Mehdian H 2008 *Nucl. Instrum. Meth. Phys. Res. A* **591** 338
[20] Rouhani M H and Maraghechi B 2009 *Phys. Plasmas* **16** 093110
[21] Rouhani M H and Maraghechi B 2010 *Phys. Plasmas* **17** 023104
[22] Ganguly A K and Freund H P 1985 *Phys. Rev. A* **32** 2275
[23] Reiche S 1999 *Nucl. Instrum. Meth. Phys. Res. A* **429** 243
[24] Lin A T and Lin C C 1986 *Nucl. Instrum. Meth. Phys. Res. A* **250** 1373
[25] Freund H P and Antonsen T M Jr 1992 *Principles of Free-Electron Lasers* (London: Chapman and Hall) chapter 5